Institute of Physics Publishing Journal of Physics: Conference Series **11** (2005) 207–222
doi:10.1088/1742-6596/11/1/021 Kinetic Theory of Nonideal Plasmas

Charged colloids and polyelectrolytes: from statics to electrokinetics

H Löwen, A Esztermann, A Wysocki, E Allahyarov, R Messina, A Jusufi, N Hoffmann, D Gottwald,* G Kahl,* M Konieczny, C N Likos

Institut für Theoretische Physik II, Heinrich-Heine-Universität Düsseldorf, Universitätsstraße 1, D-40225 Düsseldorf, Germany

*Center for Computational Materials Science and Institut für Theoretische Physik, Technische Universität Wien, Wiedner Hauptstraße 8-10, A-1040 Wien, Austria

E-mail: `hlowen@thphy.uni-duesseldorf.de`

Abstract. A review is given on recent studies of charged colloidal suspensions and polyelectrolytes both in static and non-equilibrium situations. As far as static equilibrium situations are concerned, we discuss three different problems: 1) Sedimentation density profiles in charged suspensions are shown to exhibit a stretched non-bariometric wing at large heights and binary suspensions under gravity can exhibit an analog of the brazil-nut effect known from granular matter, i.e. the heavier particles settle on top of the lighter ones. 2) Soft polyelectrolyte systems like polyelectrolyte stars and microgels show an ultra-soft effective interaction and this results into an unusual equilibrium phase diagram including reentrant melting transitions and stable open crystalline lattices. 3) The freezing transition in bilayers of confined charged suspensions is discussed and a reentrant behaviour is obtained. As far as nonequilibrium problems are concerned, we discuss an interface instability in oppositely driven colloidal mixtures and discuss possible approaches to simulate electrokinetic effects in charged suspensions.

1. Introduction

If mesoscopic silica or polystyrene particles are brought into contact with a dipolar solvent (such as water), ionic groups will dissociate into the solvent leaving back an oppositely charged surface. This charging process is schematically shown in Figure 1. The net charge arising for micron-sized colloidal spheres is huge and of the order of $Z = 1000 - 100000$ elementary charges. Therefore these particles are called "polyions" or "macroions". The microscopic ionic groups which are dissociated in the solvent are called "counterions". The fact that macroions are highly charged brings them into the class of strongly coupled Coulomb systems, a field where the late Yuri Klimontovich has brought in very originial ideas. Therefore we dedicate this paper to his memory.

The traditional approach is the so-called "primitive model" of strongly asymmetric electrolytes where the interaction between the different species is modelled by excluded volume (hard core) and Coulomb interactions. The latter are reduced by a factor $1/\epsilon$ from the bare Coulomb law where ϵ denotes the dielectric constant of the solvent. Due to the long range of the Coulomb interactions, there is a strong coupling between the ions leading to various interesting effects both in equilibrium and non-equilibrium such as overcharging, like-charge attraction and electrokinetic friction, see Refs. [1, 2, 3, 4, 5] for a review. The primitive model

© 2005 IOP Publishing Ltd

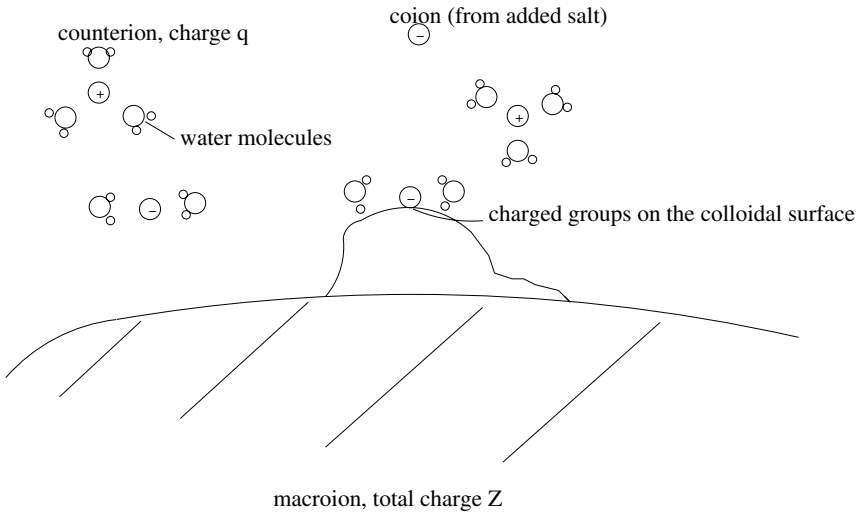

Figure 1. Sketch of charges at a macroionic surface on a molecular scale. The solvent molecules are also shown.

can also be applied to polyelectrolytes which are long flexible or rod-like chain molecules with charges along their backbone or with charged side groups. These chains can be linear or can possess more complicated architectures such as star-like polyelectrolytes or crosslinked gels. A conceptually simpler approach is based on the traditional linear screening theory of Debye and Hückel which results in a Yukawa interaction between all charged macro-particles. The screening is mediated by all the microions in the solution. If this model is applied to colloidal suspensions and polyelectrolytes, there are still a variety of novel effects.

In this paper, we shall review some recent progress in the field of charged colloidal suspensions and polyelectrolyte solutions, both for equilibrium and non-equilibrium situations. Regarding equilibrium situations we discuss first of all colloidal sedimentation equilibrium. The associated density profiles in charged suspensions are shown to exhibit a stretched non-bariometric wing at large heights with an apparent mass that is smaller than the buoyant mass of the colloidal particles. We explain this effect by counterion *entropy*. Furthermore, binary suspensions under gravity exhibit a "colloidal brazil-nut effect" similar to that known from granular matter: the heavier particles settle on top of the lighter ones provided their mass per charge is smaller than that of the lighter particles. As a second example, we consider soft polyelectrolyte systems like polyelectrolyte chains, polyelectrolyte stars and ionic microgels. These objects are governed by a penetrable effective pairwise interaction as we demonstrate explicitly for long weakly charged polyelectrolyte chains. In most cases, the dominant contribution to the pair interaction is again counterion *entropy*. The penetrability leads to an equilibrium phase diagram with unusual freezing properties including a reentrant melting transition and stable open crystalline lattices. The third and last equilibrium situation considered here is the freezing transition in bilayers of confined charged suspensions.

We then focus our attention to non-equilibrium problems. These are problems arising if an external field is applied to an equilibrium charged suspensions [6]. Here the Brownian dynamics of the suspensions becomes crucial. First an interface instability in oppositely driven colloidal mixtures is described. Then we discuss possible approaches to simulate electrokinetic problems in charged suspensions.

2. Charged colloids under gravity

2.1. One-component charged suspensions

One hundred years ago, Einstein [7] suggested to extract Boltzmann's constant k_B from the low-density wing of a colloidal sedimentation profile. In fact, Boltzmann statistics predicts an exponentially decaying number density profile $\rho(z)$ of the colloidal particles

$$\rho(z) \propto \exp(-z/\ell_g) \tag{1}$$

Here z is the height coordinate parallel to the direction of the gravitational acceleration g and

$$\ell_g \equiv k_B T/m_0 g \tag{2}$$

is the gravitational length where m_0 is the buoyant mass of a single colloidal particle and T is the system temperature assuming an isothermal sample. Hence k_B is obtained by the slope of a plot of $\ln \rho(z)$ versus z provided all the other parameters are known. Perrin [8] actually used this idea and determined k_B. An interesting deviation from the ideal bariometric law (1) was reported in 1993 using depolarized-light scattering experiments by Piazza et al [9]. In strongly deionized charged colloidal suspensions, they found still an exponential decay of the colloidal density profiles, but the associated decay length ℓ was larger than the gravitational length ℓ_g. This result can immediately be expressed in terms of an *apparent mass* m of the colloids which is smaller than the buoyant mass m_0, i.e. $m/m_0 = \ell_g/\ell < 1$.

The simplest theoretical understanding of the mass reduction is based on an *entropic lift effect* as induced by the counterions [10, 11] provided they are slaved to the macroions due to the strong Coulomb coupling. Suppose the system is salt-free and the Coulomb coupling is so strong that the system is locally electroneutral. The latter assumption implies that the inhomogeneous counterion density $\rho_c(z)$ is enslaved to the macroion density $\rho_m(z)$ via the constraint

$$q\rho_c(z) = Z\rho_m(z) \tag{3}$$

where q is the counterion valency and Z is the macroion charge. The counterion entropy will tend to delocalize the macroions. A straightforward density functional calculation then yields

$$m/m_0 = 1/(Z/q + 1). \tag{4}$$

This may be called an entropic lifting effect. A more detailed treatment including the effect of added salt was done by Löwen [11] and van Roij [12]. In the latter work even density profiles $\rho_m(z)$ linear in z and the existence of a macroscopic electric field through the sample counteracting gravity were predicted. This field was confirmed in recent experiments [13]. Computer simulations of the primitive model, on the other hand, were also used to predict the colloidal density profiles. They reveal again a macroscopic electric field through the sample [14]. Other simulations [15] confirm the result for the apparent mass m as obtained via the density functional approach of Ref.[11].

A still open question is the effect of an external static field on the sedimentation profiles of a charged suspensions. If the field counterbalances gravity, an interesting question is when and how, the colloidal density profile delocalizes as revealed, e.g., by a divergent sedimentation height

$$h = \int_0^\infty dz\ \rho_m(z) z. \tag{5}$$

Based on Poisson-Boltzmann theory, delocalization transition (i.e. $h \to \infty$) is expected when the external electric field approaches the critical strength

$$E_c = m_0 g/|Ze|. \tag{6}$$

2.2. Colloidal "brazil nut" effect

Let us now discuss sedimentation of *binary* charged suspensions. Here we focus on an effect which is similar to granular systems: Upon shaking binary granular grains in gravity the larger particles lie on top of the smaller ones even if they are heavier and denser than the small ones. This is due to a sifting mechanism in which tiny grains filter through the interstices between the large particles well-known as "brazil-nut" effect: in a jar of mixed nuts or in a cereal package, the largest species rises to the top [16, 17].

Recently, in Ref. [15], equilibrium density profiles of binary charged colloidal fluids under gravity were calculated based on computer simulations of the primitive model and using density functional theory. It was predicted that the heavier particles sediment on top of the lighter ones provided they are very highly charged. In analogy to granular matter, this counter-intuitive effect was called *colloidal brazil-nut effect*. Again it is generated by the entropy of the microscopic counterions in the solution which are coupled to the macroions by strong Coulomb binding. In fact, it is the ratio of buoyant mass per colloidal charge which controlls the efficiency of the effect: the species with the smallest α is lifted most. Density functional theory predicts that a brazil nut effect occurs at

$$\frac{m_1}{Z_1/q+1} = \frac{m_2}{Z_2/q+1} \tag{7}$$

where Z_1, Z_2 and m_1, m_2 are the charge numbers and the buoyant masses of the two species and q is the counterion charge. This finding was supported by extensive Monte Carlo computer simulations of the primitive model. Simulation results for the colloidal and counterion densities are shown in Figure 2 confirming the criterion (7). Although the first species is heavier than the second one, its averaged height is much larger than that of the second species in the case $Z_1 = 45$. It has also be shown in Ref. [15] that the brazil nut effect is stable with respect to addition of salt but the overall salt concentration has to be relatively small.

The brazil nut effect is predicted only in the wings. For finite densities at lower height of the sediment, however, Archimedes' law applied to an effective volume set by the strength of the interaction will also lead to a similar trend. Therefore it should be possible to see the brazil-nut effect experimentally.

3. Polyelectrolytes with ultrasoft interactions: equilibrium properties

3.1. Effective interactions between weakly charged linear polyelectrolyte chains

As a first example, we briefly discuss weakly charged linear polyelectrolyte chains. Results for the effective forces as a function of their mutual centre-of-mass separation D are presented in Figure3. The effective potentials obtained are ultrasoft and bounded for vanishing center-of-mass distances but nevertheless much more repulsive than those obtained for polymer chains. The physical reasons lie both in the electrostatic repulsion between the charges carried on the chains and in the entropically caused osmotic pressure of the counterions that are trapped within the interior of the chains. The effective potential includes an explicit density dependence arising from the redistribution of counterions inside and outside the chains upon a change of the overall concentration. The data can very well be described by a Gaussian form in agreement with a theoretical mean-field model [18].

3.2. Freezing in polyelectrolyte star solutions

Let us now discuss highly charged and star-like polyelectrolytes. Pioneering work on star-shaped polyelectrolytes ("porcupines") goes back to Pincus [19], who predicted that the force between two polyelectrolyte stars should be dominated by the *entropic* contribution of the counterions. Jusufi and coworkes used molecular Dynamics computer simulations of monomer resolved models and put forward a variational theory to study the sizes, conformations and interactions of polyelectrolyte stars for high charging fractions [20, 21]. An analytical expression of the effective

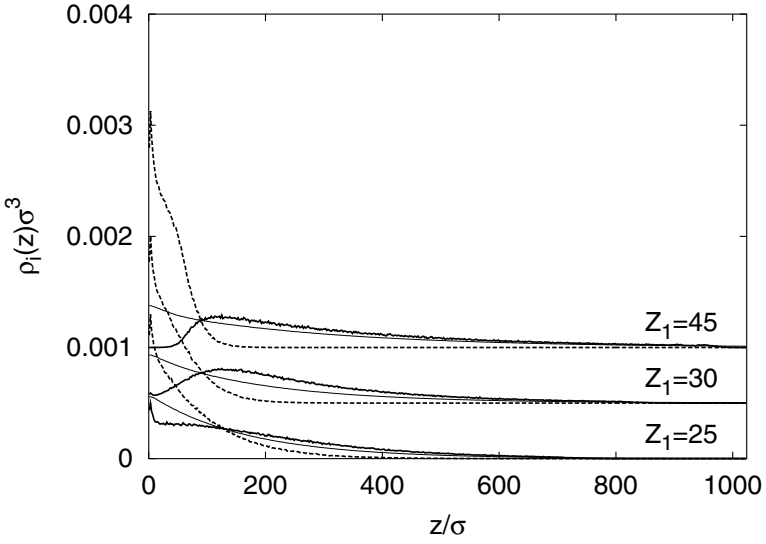

Figure 2. Density profiles of macro- and counterions for $Z_1 = 45, 30, 25$ (solid lines; top to bottom). The second colloidal component is shown as a dashed line. Counterion densities (thin lines) have been divided by $Z_1 + Z_2$. For clarity, curves pertaining to different simulation runs have been shifted by 5×10^{-4} with respect to each other. The parameters are: $m_1/m_2 = 1.5$, $Z_2 = 15$, $\ell_2/\sigma = 10$, with ℓ_2 denoting the gravitational length of the second species and σ denoting the hard core diameter of the two species. Furthermore the Bjerrum length is $\lambda_B = \sigma/128$ and the partial densities per area of both colloidal species are $0.1/\sigma^2$. There is no added salt. From Ref. [15].

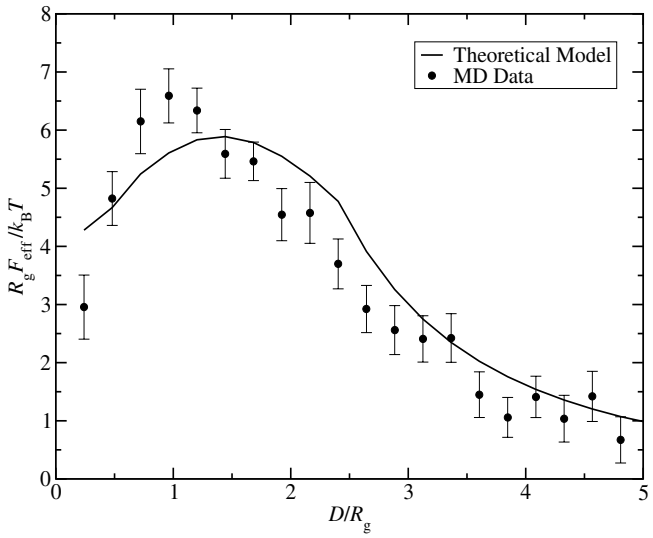

Figure 3. Effective force $F_{\rm eff}(D)$ acting on the center-of-mass of a polyelectrolyte chain as a function of the interchain separation D scaled by the radius of gyration R_g of a single chain. The results shown here pertain to chains with $N = 100$ monomers each and charging fraction $\alpha = 0.10$, i.e., every tenth monomer is charged. The solid line represents a mean-field theoretical prediction, whereas points denote corresponding computer simulation data. From Ref. [18].

interactions between two polyelectrolyte stars obtained by the theory was confirmed by the simulations. A further analysis of the analytical expression [22] revealed that the old argument of Pincus was right: the interactions we mainly dominated by the entropy of the counterions which are confined in the dumbbell-shaped region between two overlapping polyelectrolyte stars. As a consequence, the interaction is very soft, it is even bounded for complete overlap. The physical origin of the soft interaction, however, is different from that discussed in the previous chapter. One caveat one has to keep in mind, is that the interaction is density dependent, similar to the classic Debye-Hückel resp. Derjaguin-Landau-Verwey-Overbeek result [1].

The full phase diagram of a star-shaped polyelectrolyte solution has also been calculated [23] based on liquid-integral theory for the fluid and harmonic theory of different crystalline solids. The result is presented in Figure 4 in the plane spanned by the arm number f and the number density ρ_s of the stars. Two features are worth to be mentioned. First there is a *reentrant melting effect* for increasing density and a fixed arm number f of about 15. There is first freezing into an fcc lattice which transfoms into a *bcc* lattice and then melts again. There is a further reentrant melting with an intermediate *bcc* solid. Second, for large densities a wealth of *open and exotic lattices* are getting stable such as body-centered othogonal lattices, hexagonal stacks, simple cubic lattices and a diamond lattice. The latter is of importance to fabricate optical band-gap materials (photonic crystals). The common wisdom is that steep interactions exhibit freezing into an fcc lattice and soft interactions - as the one-component plasma with a neutralizing homogeneous backgroud - freeze into *bcc* crystals. For ultrasoft interactions, the lesson to be learned from Ref. [23] and from studies with similar soft potentials [24, 25], is that more open crystal lattices get thermodynamically stable. An experimental verification of this phase diagram is still needed.

3.3. Freezing in ionic microgels

A further example where soft interactions lead to reentrant melting and stable open crystal structure are ionic microgels. We consider the case of spherical and weakly crosslinked but highly charged gels. Their effective interaction is governed by the screened electrostatics. The simplest approach to the effective interactions was discussed by Denton [26] and assumes homogeneously charged spheres which are penetrable. Linear screening theory produces the pair interactions as a convolution with the Yukawa kernel. The Fourier transform of the effective pair interaction $V(r)$ is then

$$\tilde{v}_{\rm ind}(k) = -\frac{36\prod Z^2e^2}{\epsilon}\frac{\kappa^2}{k^6a^4(k^2+\kappa^2)}\left[\cos(ka) - \frac{\sin(ka)}{ka}\right]^2 .$$

Here, Ze is the net microgel charge with the electron charge e, ϵ is the dielectric constant of the solvent, $a = \sigma/2$ is the particle radius and $\kappa = \sqrt{4\prod n_c z^2 \lambda_{\rm B}}$ is the inverse Debye screening length from the counterions of density n_c and valency z. We will consider monovalent microions in what follows and then their density n_c is related to the microgel density ρ via the global electroneutrality. Finally, $\lambda_{\rm B} = 7.1\mathring{A}$ is the Bjerrum length. Note that the interaction is again density dependent via the κ parameter.

The phase diagram was theoretically calculated in Ref. [27]. An example is shown in Figure 5 where the phases are plotted for different microgels charges Z as a function of the microgel number density ρ scaled with the inverse cube of their diameter $\sigma = 2a$. Again there is reentrant melting for increasing density ρ at fixed total charge Z for $Z \approx 250$. And again, there are many stable open lattice structures including now a trigonal low-symmetry structure which intervenes between two body-centered orthogonal (bcs) structures of different anisotropies.

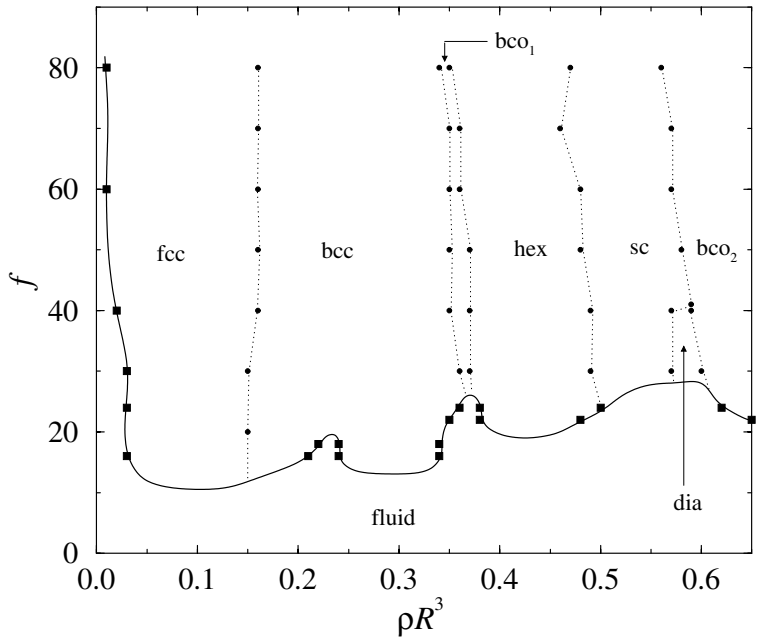

Figure 4. Phase diagram of a polyelectrolyte star solution versus number density of the stars ρ_s scaled with the corona radius R and versus arm number f. The charging fraction of the monomers is 1/3. The Bjerrum length is fixed to $\lambda_B = 7.1\mathring{A}$. There is no added salt. The points denotes the phase coexistence between different crystal structures: apart from the fluid, there are stable face-centered cubic (*fcc*), body centered cubic (*bcc*), body-centered-othogonal (*bco*), hexagonally stacked (*hex*), simple cubic (*sc*), and diamond (*dia*) lattices. The squares denote solid fluid transitions, the density gaps of the coexistence region are extremely small and not resolved. The lines are guides to the eye. From Ref. [23].

3.4. Intuitive argument for reentrant melting and stable open lattices

Let us finally present a simple intuitive argument for the reentrant melting transition and the stability of an open crystalline lattice. The typical shape of an ultrasoft effective interaction potential needed to exhibit reentrant melting and stable open lattices has two ingredients, namely a soft core and a separation distance (corona) σ above which the interaction is small. A linear ramp potential, as sketched in Figure 6 , is one simple possible representative of this class.

Reentrant melting can be explained intuitively as follows, see Figure 6a: an increasing number density ρ means that the mean interparticle spacing a_N, i.e. the nearest neighbour distance, is decreasing as $a_N \approx \rho^{-1/3}$. For low density (corresponding to large a_N), the system is fluid, since the repulsive interaction felt in the cage of neighbours is relatively small. Increasing the density ρ, a_N will reach σ from above where the system feels the strongly increasing repulsion. This results in a freezing transition into a periodic lattice. Increasing the density ρ further, the particle will softly penetrate each other, but the repulsive energetic penalty for penetration is relatively weak. At the certain neighbour distance smaller than σ the system will realize this and remelt again in order to increase its entropy again. This explains reentrant melting.

The stability of exotic open crystal lattices, on the other hand, is explained by discussing simple lattice sums of the total potential energy. This corresponds to a zero temperature ($T = 0$) consideration. Different lattice structures compete in their total potential energy and

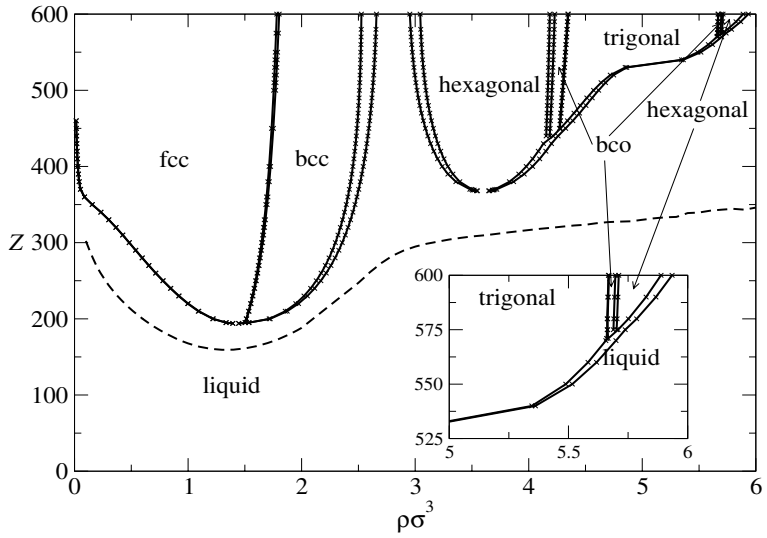

Figure 5. The phase diagram of ionic microgels with diameter $\sigma = 100\,\mathrm{nm}$. The crosses denote calculated phase boundaries whereas the lines are guides to the eye connecting these points. The unlabeled narrow regions between phases denote domains of phase coexistence (density jumps), whereas the dashed line is the locus of points in which the highest peak of $S(k)$ attains the Hansen-Verlet value 2.85. The inset shows the high-density, high-charge part in more detail. From Ref. [27].

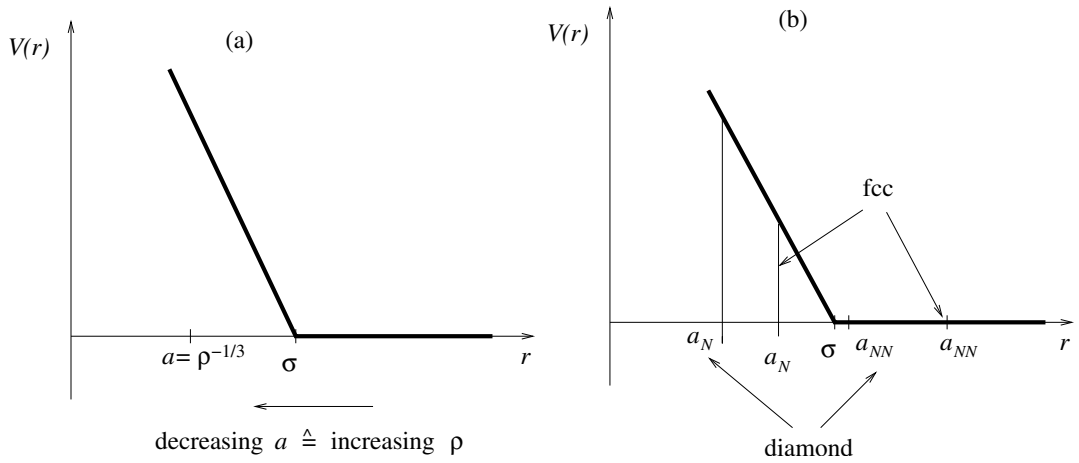

Figure 6. Intuitive arguments for a) reentrant melting, and b) stable open crystals. The pair potential $V(r)$ is shown as a linear ramp with cut-off at the corona diameter σ. The corresponding distances a, a_N, and a_{NN} are also indicated both for a closed structure (fcc) and an open strcture (diamond).

	fcc	bcc	sc	$diamond$
$a_{\rm N}\rho^{1/3}$	$4^{1/3}/\sqrt{2}$	$2^{-2/3}\sqrt{3}$	1	$8/\sqrt{3}$
$a_{\rm NN}\rho^{1/3}$	$4^{1/3}$	$2^{1/3}$	$\sqrt{2}$	$2\sqrt{2}$
$a_{\rm NNN}\rho^{1/3}$	$4^{1/3}\sqrt{2}$	$2^{1/3}\sqrt{2}$	$\sqrt{3}$	2
$N_{\rm N}$	12	8	6	4
$N_{\rm NN}$	6	6	12	12
$N_{\rm NNN}$	24	12	8	12

Table 1. The first three nearest neighbour distances $a_{\rm N}$, $a_{\rm NN}$, and $a_{\rm NNN}$, reduced by $\rho^{-1/3}$ and the numbers, $N_{\rm N}$, $N_{\rm NN}$, and $N_{\rm NNN}$, of the first three neighbour shells for four different lattices fcc, bcc, sc, $diamond$.

the structure that minimizes the potential energy per particle for a prescribed density will be the stable phase. The lattice-sum potential energy U/N per particle reads

$$U/N = \frac{1}{2}[N_N V(a_N) + N_{NN} V(a_{NN}) + N_{NNN} V(a_{NNN}) + ...] \qquad (XXX)$$

The factor 1/2 avoids double-counting and a_N is the neighbour distance while $a_{\rm NN}$ resp. $a_{\rm NNN}$ are the next nearest neighbour resp. the third nearest neighbour distance. They all scale with the prescribed number density ρ as $\rho^{-1/3}$. Correspondingly the positive integer numbers $N_{\rm N}$, $N_{\rm NN}$ and $N_{\rm NNN}$ denote the number the nearest, next nearest and third-order neighbours. All these quantities depend on the lattice chosen as summarized in Table 1.

Now the actual value of the lattice sums applied to a soft-core potential depends crucially on the density. Let us discuss, for example, the case of an fcc lattice and a diamond structure, see Figure 6b. If the density is such that the next nearest neighbours of the diamond structure are kept out of the corona, the only contribution in the lattice sum (XXX) comes from the first neighbours. Although $a_{\rm N}$ is smaller in the diamond phase than in the fcc lattice, this is more than compensated by the prefactor $N_{\rm N}$ which is 4 for diamond and 12 for fcc. For steep repulsions this is completely different as the sharp increase in $V(r)$ makes an open lattice less favorable. However, for ultrasoft potentials with a corona, there is a density window where an open lattice (such as diamond) can get stable.

4. Freezing in bilayers of Yukawa particles

Let us now focus on phase behaviour in *confined* charged suspensions. A typical confinement is achieved when the colloidal particles are between two narrows glass plates in a slit or wedge geometry. As one knows from the phase diagram of neutral hard spheres between two neutral plates, the crystalline phases exhibits layering and prism superlattices and there is a subtle dependence on the plates distance [28, 29, 30, 31].

Recently the phase diagram was calculated for bilayers assuming a Yukawa pair interaction $V(r) \propto \exp(-\kappa r)/r$ [32] for zero temperature. This is an appropriate model for charged colloid or dusty plasmas [33, 34]. Five different nested bilayers crystalline structures were considered. These are summarized in Table 2. The phase diagram which is shown in Figure 7 depends on two length scale ratios, λ and η. Using the bilayer distance D, we define $\lambda = \kappa D$ and $\eta = \rho D^2/2$ where ρ is now the number density per area.

The phase diagram shown in Figure 7 is *not* a simple interpolation between the hard sphere case ($\lambda \to \infty$) and the confined plasma ($\lambda \to 0$). The confined plasma was discussed earlier in Refs. [35, 36]. There is a *reentrant behavior* of the IVA phase at fixed density upon varying λ as indicated in Fig. 7 by the vertical arrow. This can in principle be confirmed in experiments on charged suspensions as a function of added salt concentration [31].

Phase	$\mathbf{a}_2/a_1$	$\mathbf{c}$	$\rho a_1^2/2$
I. Rectangular	$(0,\sqrt{3})$	$(\mathbf{a}_1+\mathbf{a}_2)/2$	$1/\sqrt{3}$
II. Rectangular	$(0,\gamma)$	$(\mathbf{a}_1+\mathbf{a}_2)/2$	γ
III. Square	$(0,1)$	$(\mathbf{a}_1+\mathbf{a}_2)/2$	1
IV. Rhombic	$(\cos\theta,\sin\theta)$	$(\mathbf{a}_1+\mathbf{a}_2)\alpha$	$1/\sin\theta$
V. Triangular	$(1/2,\sqrt{3}/2)$	$(\mathbf{a}_1+\mathbf{a}_2)/3$	$2/\sqrt{3}$

Table 2. Structure and parameters of the different staggered bilayer crystals. $\mathbf{a}_1$ is set to $(a_1,0)$ where a_1 is the nearest intralayer distance between particles. For phase II, $\gamma = a_2/a_1$ is the aspect ratio. For phase IV, θ is the angle between $\mathbf{a}_1$ and $\mathbf{a}_2$, and α is a free parameter characterizing the relative lateral interlattice shift $\mathbf{c}$. From Ref. [32].

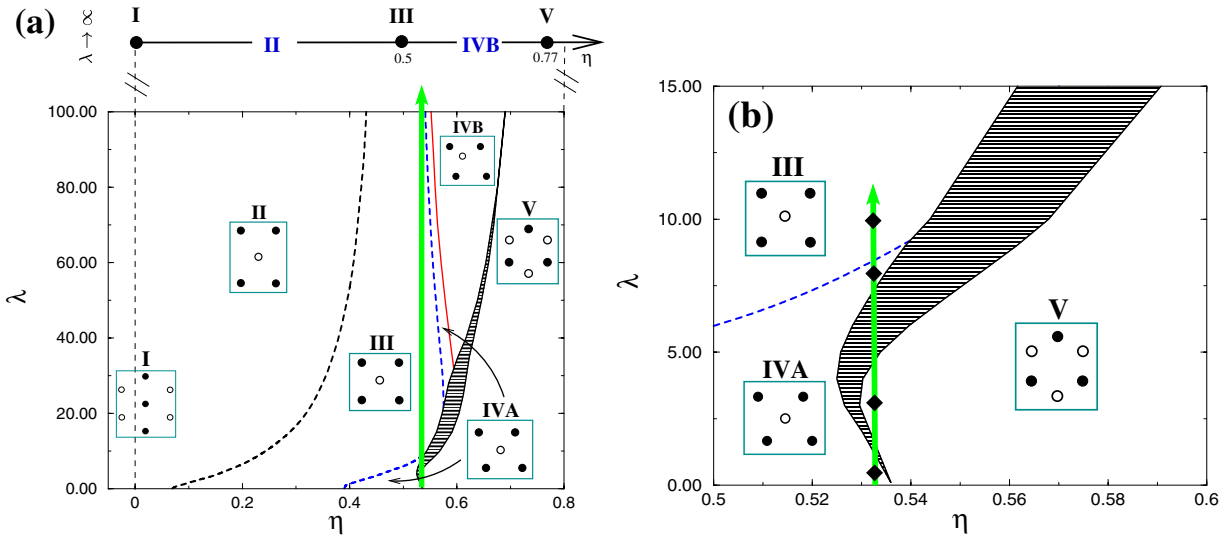

Figure 7. Phase diagram of the Yukawa bilayer in the (η,λ) plane. (a) The hard sphere limit $\lambda \to \infty$ is sketched on top. The dashed (solid) lines denote continuous (discontinuous) transitions. The filled region corresponds to the coexistence domain of phases IV and V. The tiny phase coexistence domain of phases IVA and IVB is thinner than the IVA/IVB boundary line. Phase I appears only at extremely low η values and is not reported here. The vertical arrow indicates the *double* reentrant behavior of phase IVA. The insets show the lattice geometries, where the filled (open) circles correspond to the lower (upper) layer. (b) Magnification of (a) showing a reentrant behavior of phase IVA occurring at moderate λ. The four diamonds along the arrow indicate state points which were investigated by computer simulation at finite temperatures. From Ref. [32].

5. Interface instability in oppositely driven colloidal mixtures

When binary mixtures of charged colloidal particles are driven by an external field, as e.g. gravity or an electric field, they form particle lanes provided the external strength of the drive is high enough. This was shown in nonequilibrium Brownian dynamics computer simulations [37, 38, 39] and by theory [40, 41]. The direction of the lanes is along the driving force direction. Typically the starting configuration is a completely mixed state.

Here we focus on another starting configuration namely a completely demixed state. Such a situation may be experimentally achieved in colloid-polymer mixtures [42]. The data published here are new and have some relevance in interpreting the Rayleigh Taylor instability without

surface tension. For a finite surface tension, similar data have been published in [43].

We consider a two-dimensional model system interacting via a set of Yukawa pair potentials. The asymmetric binary colloidal mixture comprises $N_1 + N_2$ Brownian colloidal particles in an area S [37]. N_1 particles are of type 1, the other N_2 are of type 2 with partial number densities $\rho_1 = N_1/S$ and $\rho_2 = N_2/S$. In the following we set $\rho_1 = \rho_2 = \rho$. The colloidal suspension is held at fixed temperature T via the bath of microscopic solvent particles. Two colloidal particles are interacting via effective Yukawa potentials as follows:

$$\frac{V(r)}{k_B T} = U_0\,\sigma \frac{\exp(-\kappa(r-\sigma))}{r}. \tag{8}$$

Here r is the center-to-center separation, U_0 is the interaction strength measured in terms of the thermal energy $k_B T$ and κ is the inverse screening length and σ is a further length scale.

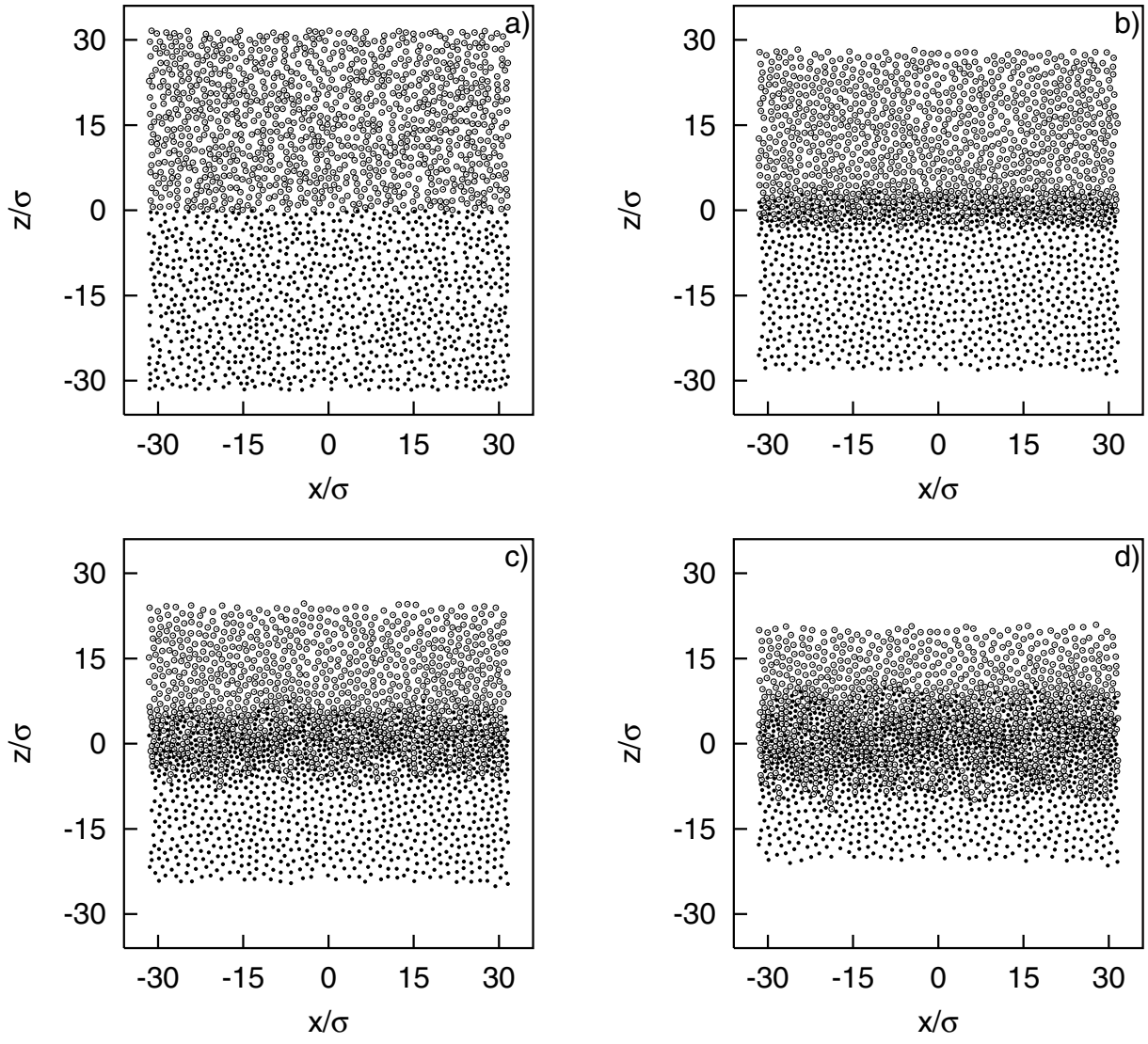

Figure 8. Simulation snapshots for a) $t = 0\,\tau_B$, b) $t = 0.45\tau_B$, c) $t = 0.9\tau_B$, d) $t = 1.35\tau_B$. Simulation parameters are: $\kappa\sigma = 3$, $U_0 = 10$, $\frac{F\sigma}{k_B T} = 90$, $\rho\sigma^2 = 0.5$, $N_1 = N_2 = 1000$, $\Delta = 0$

The dynamics of the colloids is completely overdamped Brownian motion. The friction constant is $\xi = 3\pi\eta\sigma$ with η denoting the shear viscosity of the solvent. The constant external force acting on the ith particle of species j, $\vec{F}_i^{(j)}$, has the same amplitude but an opposite direction for the both constituents of the binary mixture. It is $\vec{F}_i^{(1)} = F\vec{e}_y$ and $\vec{F}_i^{(2)} = -F\vec{e}_y$ where $\vec{e}_y$ is a unit vector along the y-direction of the system.

The stochastic Langevin equations for the colloidal trajectories $\vec{r}_i^{(j)}(t)$ $(j = 1, 2)$ (with $i = 1, ..., N_1$ for $j = 1$ and $i = 1, ..., N_2$ for $j = 2$) read as

$$\xi \frac{d\vec{r}_i^{(j)}}{dt} = -\vec{\nabla}_{\vec{r}_i^{(j)}} [\sum_{k=1}^{N_{j'}} V(\mid \vec{r}_i^{(j)} - \vec{r}_k^{(j')} \mid) + \sum_{k=1, k\neq i}^{N_j} V(\mid \vec{r}_i^{(j)} - \vec{r}_k^{(j)} \mid)] + \vec{F}_i^{(j)} + \vec{K}_i^{(j)}(t), \tag{9}$$

where j' is the complementary index to j ($j' = 1$ if $j = 2$ and $j' = 2$ if $j = 1$). The right-hand-side includes all forces acting onto the colloidal particles, namely the force resulting from inter-particle interactions, the external constant force, and the random forces $\vec{K}_i^{(j)}$ describing the collisions of the solvent molecules with the ith colloidal particle of species j. The latter are Gaussian random numbers with zero mean, $\overline{\vec{K}_i^{(j)}} = 0$, and variance

$$\overline{(\vec{K}_i^{(k)})_\alpha(t)(\vec{K}_j^{(n)})_\beta(t')} = 2k_BT\xi\delta_{\alpha\beta}\delta_{ij}\delta_{kn}\delta(t - t'). \tag{10}$$

The subscripts α and β stand for the two Cartesian components. Note that within this simple Langevin picture, hydrodynamic interactions are ignored.

We solve the Langevin equations of motion by Brownian dynamics simulations [44, 45, 46] using a finite time-step and the technique of Ermak [47, 48]. We use a square cell of length ℓ with periodic boundary conditions. The typical size of the time-step Δt was $0.003\tau_{\rm B}$, where $\tau_B = \xi\sigma^2/k_BT$ is a suitable Brownian timescale. We simulated typically 500 time steps which corresponds to a simulation time of $1.5\tau_B$.

A set of different snapshots are presented in Figure 8 for different times. The starting configuration at $t = 0$ (see Fig. 8.a) is a completely demixed configuration. One clearly sees the onset of an interfacial instability upon a strong drive such that particles driven alike form lanes which are penetrating eachother.

6. Simulating electrokinetic effects

Nonequilibrium effects in charged suspensions require a realistic description of the dynamics both for the macroions and the microions. In particular, *hydrodynamic* interactions mediated via the solvent when the macro- and microions are moving are getting important resulting in electrokinetic effects. Hydrodynamical interactions are completely irrelevant for equilibrium properties and were therefore not considered in the previous considerations of equilibrium structure and phase diagrams.

Significant progress has been made in the last decade in studying the hydrodynamics of many neutral colloids either by discrete lattice-Boltzmann methods, continuum solvent models, or dissipative particle dynamics [49]. A special method was proposed by Tanaka and Araki in Ref. [50]: quite complementary to lattice-Boltzmann methods where the fluid solvent is put on a "solid" grid, in the ulimit: Command not found.

Tanaka-Araki method the solid particle is modelled as a highly viscous fluid. This "fluidization method" avoids the numerically costly non-slip boundary condition at the colloidal surfaces and provides an efficient computation of dynamical phenomena.

The hard problem is to include both explicit ions and hydrodynamics on the same level combining electrostatics for the microions and hydrodynamics for the solvent. One obvious

escape route is to simulate macroions, microions and explicit solvent (as e.g. water within the SPC/E interaction) by molecular dynamics. Recent progress has been made by Dzubiella and Hansen [51] but certainly only small macroparticles size (appropriate for proteins) can be treated on present-day computers. A complementary strategy (more appropriate for microsized colloids) is to stick to a mesoscale treatment of the solvent flow and to couple this dynamically to the ion density field. One of the recent attempts based on lattice-Boltzmann approaches was proposed by He and Li [52] assuming local charge neutrality. A different lattice-Boltzmann approach with an additional charge density field was introduced by Warren [53] and later technically improved by Horbach and Frenkel [54] and by Capuani and coworkers [55].

Recently, two further approaches were proposed: Kodama and coworkers [56] have proposed another approach which is based on the "fluidization method" [50] of the solid colloidal particles. The electrostatics of the microions is described on the level of Poisson-Boltzmann theory. Kodama *et al* then consistently couple the diffusive dynamics of the microion density field (including added salt) to the hydrodynamics of the solvent flow. They were able to solve a *full dynamical problem* of electro-deposition of charged colloids near a charged planar substrate. Second, Lobaskin and Dünweg [57] proposed an efficient hybrid lattice Boltzmann and Langevin molecular dynamics scheme which is designed for charged suspensions as well [58].

Other interesting problems of charged colloidal dynamics are electrophoresis [59], electrolyte friction [60], conductivity in suspensions driven by an electric field [62, 63] and crystal nucleation and growth [61, 64]. With similar techniques are described above [52, 53, 54, 56] it should be possible to tackle these problems in the near future.

7. Conclusions

While equilibrium situations are by now well-understood for simple systems, there are still many fascinating open questions for complex fluids. We have shown examples as sedimentation density wings in charged suspensions and very rich equilibrium freezing diagrams for systems governed by ultrasoft interactions.

On the other hand, if simple systems are brought into nonequilibrium, such as charged colloidal dispersions in external fields, genuine non-equilibrium effects arise which require a more sophisticated theoretical treatment. The next decades will see much more efforts (and hopefully progress) in this area. The relevant reserach directions can be classified according to the complexity diagram shown in Figure 9 which provides a road-map of complexity. On the x-axis system complexity is shown while there is another kind of complexity, namely the complexity of the question posed, shown at the y-axis. On the one hand, system complexity is related to the statistical degrees of freedom present in the system. The simplest case are spherical particles while mixtures and orientational degrees of freedom represent a higher level of system complexity. On the other hand, the complexity of the question asked can comprise equilibrium situations, such as inhomogeneous systems near walls and in restricted geometries, steady-state non-equilibrium cases such as systems under permanent shear flow or other time-independent or oscillatory external fields. Finally, full non-equilibrium situations arise if a field is turned on or switched off.

The research routes which can be followed are shown as arrows schematically in Figure 9. We anticipate that the next decades will reveal a wealth of interesting physics in this interdisciplinary domaine.

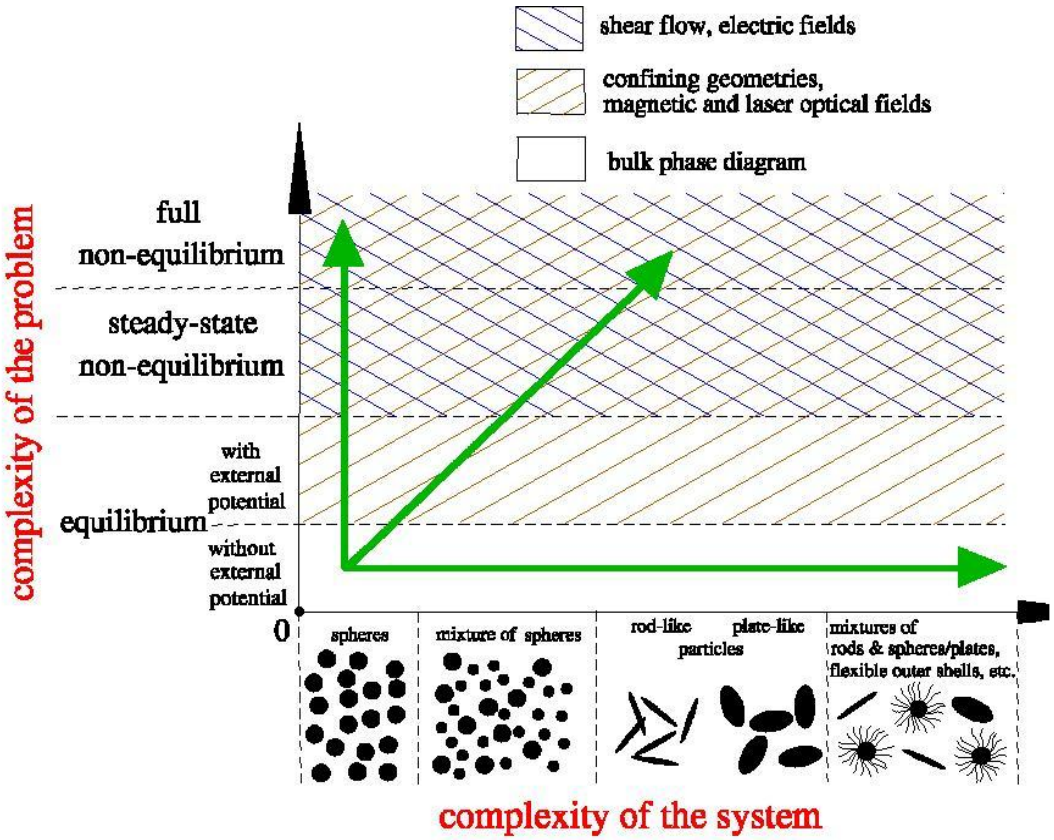

Figure 9. Classification of complexity and main research routes in the research field of colloidal dispersions in external fields. From Ref. [6].

Acknowledgments
We thank Assoud Lahcen for typing the manuscript. Financial support from the DFG (Sonderforschungsbereich TR6 subproject D1) is gratefully acknowledged. We dedicate this paper to the memory of Yuri Klimontovich.

References

[1] J.-P. Hansen, H. Löwen, Annual Reviews of Physical Chemistry, **51**, 209 (2000).
[2] J.-P. Hansen, H. Löwen, *Effective interactions for large-scale simulations of complex fluids,* Springer Series, edited by P. Nielaba et al, 2003.
[3] L. Belloni, J. Phys.: Condensed Matter **12**, R549 (2000).
[4] M. Dijkstra, Current Opinion in Colloid and Interface Science **6**, 372 (2001).
[5] H. Löwen, E. Allahyarov, C. N. Likos, R. Blaak, J. Dzubiella, A. Jusufi, N. Hoffmann, H. M. Harreis, J. Phys. A: Math. Gen. **36**, 5827 (2003).
[6] H. Löwen, J. Phys.: Condensed Matter **13**, R415 (2001).
[7] A. Einstein, Annalen der Physik **17**, 549 (1905); **19**, 371 (1906).
[8] J. Perrin, J. Physique **9**, 5 (1910).
[9] R. Piazza, T. Bellini, V. Degiorgio, Phys. Rev. Lett. **71**, 4267 (1993).
[10] J.-P. Simonin, J. Phys. Chem. **99**, 1577 (1995).
[11] H. Löwen, J. Phys.: Condensed Matter **10**, L479 (1998).
[12] R. van Roij, J. Phys.: Condens. Matter **15** S3569 (2003).
[13] M. Rasa, A. P. Philipse, Nature **429**, 857 (2004).
[14] A.-P. Hynninen, R. van Roij, M. Dijkstra, Europhys. Letters **65**, 719 (2004).
[15] A. Esztermann, H. Löwen, Europhys. Letters **68**, 120 (2004).
[16] J. C. Williams, Powder Technol. **15**, 245 (1976).
[17] A. Rosato, K. J. Strandburg, F. Prinz, R. H. Swendsen, Phys. Rev. Lett. **58**, 1038 (1987).
[18] M. Konieczny, C. N. Likos, and H. Löwen, J. Chem. Phys. **121**, 4913 (2004) .
[19] P. Pincus, Macromolecules **24**, 2912 (1991).
[20] A. Jusufi, C. N. Likos, H. Löwen, Phys. Rev. Letters **88**, 018301 (2002).
[21] A. Jusufi, C. N. Likos, H. Löwen, J. Chem. Phys. **116**, 11011 (2002).
[22] A. Jusufi, C. N. Likos, M. Ballauff, Colloid and Polymer Science **282**, 910 (2004).
[23] N. Hoffmann, C. N. Likos, H. Löwen, J. Chem. Phys. **121**, 7009 (2004).
[24] C. N. Likos, H. Löwen, M. Watzlawek, B. Abbas, O. Jucknischke, J. Allgaier, D. Richter, Phys. Rev. Letters **80**, 4450 (1998).
[25] M. Watzlawek, C. N. Likos, H. Löwen, Phys. Rev. Letters. **82**, 5289 (1999).
[26] A. R. Denton, Phys. Rev. E **67**, 011804 (2003).
[27] D. Gottwald, C. N. Likos, G. Kahl, H. Löwen, Phys. Rev. Letters **92**, 068301 (2004).
[28] C. A. Murray, W. O. Sprenger, and R. A. Wenk, Phys. Rev. B **42**, 688 (1990).
[29] P. Pieranski and L. Strzelecki, Phys. Rev. Lett. **50**, 331 (1983).
[30] M. Schmidt, H. Löwen, Phys. Rev. Lett. **76**, 4552 (1996); Phys. Rev. E **55**, 7228 (1997).
[31] S. Neser, C. Bechinger, P. Leiderer, T. Palberg, Phys. Rev. Lett. **79**, 2348 (1997).
[32] R. Messina, H. Löwen, Phys. Rev. Lett **91**, 146101 (2003).
[33] M. O. Robbins, K. Kremer, G. S. Grest, J. Chem. Phys. **88**, 3286 (1988).
[34] S. Nunomura, J. Goree, S. Hu, X. Wang, A. Bhattacharjee, K. Avinash, Phys. Rev. Lett. **89**, 035001 (2002).
[35] G. Goldoni and F. M. Peeters, Phys. Rev. B **53**, 4591 (1996).
[36] I. V. Schweigert, V. A. Schweigert and F. M. Peeters, Phys. Rev. Lett. **82**, 5293 (1999); Phys. Rev. B **60**, 14665 (1999).
[37] Dzubiella, J., Hoffmann, G. P., and Löwen, H., *Phys. Rev. E* **65**, 021402 (1-6) (2002).
[38] Dzubiella, J., and Löwen, H., *J. Phys.: Condensed Matter* **14**, 9383-9395 (2002).
[39] Löwen, H., and Dzubiella, J., *Faraday Discussion* **123**, 99-105 (2003).
[40] Chakrabarti, J., Dzubiella, J., and Löwen, H., *Europhys. Letters* **61**, 415-422 (2003).
[41] Chakrabarti, J., Dzubiella, J., and Löwen, H., *Phys. Rev. E* **70**, 012401 (2004).
[42] Aarts, D. G. A. L., van der Wiel, J. H., and Lekkerkerker, H. N. W., *J. Phys.: Condensed Matter* **15**, S245 (2003).
[43] Wysocki, A., and Löwen, H., J. Phys.: Condensed Matter. **16**, 7209 (2004).
[44] Hoffmann, G. P., and Löwen, H., *Phys. Rev. E* **60**, 3009 (1999).
[45] Hoffmann, G. P., and Löwen, H., *J. Phys.: Condens. Matter* **12**, 7359 (2000).
[46] Löwen, H., Hansen, J. P., and Roux, J. N., *Phys. Rev. A* **44**, 1169 (1991).
[47] Allen, M. P., and Tildesley, D. J., *Computer Simulations of Liquids*, Clarendon Press, Oxford, 1989.

[48] Ermak, D. L., *J. Chem. Phys* **62**, 4189 (1975).
[49] See, for example, the two following special issues: International Journal of Modern Physics C **9**, Number 8 (1998); Journal of Statistical Physics **107**, Numbers 1/2 (2002).
[50] H. Tanaka, T. Araki, Phys. Rev. Lett. **85**, 1338 (2000).
[51] J. Dzubiella, J.-P. Hansen, J. Chem. Phys. **119**, 12049 (2003).
[52] X. He, N. Li, Comput. Phys. Commun. **129**, 158 (2000).
[53] P. B. Warren, Int. J. Mod. Phys. C **8**, 889 (1997).
[54] J. Horbach. D. Frenkel, Phy. Rev. E **64**, 061507 (2001).
[55] F. Capuani, I. Pagonabarraga, and D. Frenkel, J. Chem. Phys. **121**, 973 (2004)
[56] H. Kodama, K. Takeshita, T. Araki, H. Tanaka, J. Phys.: Condensed Matter, **16**, L 115 (2004).
[57] V. Lobaskin, B. Dünweg, New Journal of Physics **6**, Art. No. 54 (2004).
[58] V. Lobaskin, B. Dünnweg, C. Hohn, J. Phys.: Condensed Matter **16**, S4063 (2004).
[59] M. Medebach, T. Palberg, J. Chem. Phys. **119**, 3360 (2003).
[60] R. R. Netz, Phys. Rev. Lett. **91**, 138101 (2003).
[61] M. McPhie, G. Nägele, J. Phys.: Condensed Matter **16**, S4021 (2004).
[62] P. Wette, H. J. Schöpe, R. Biehl, T. Palberg, J. Chem. Phys. **114**, 7556 (2001).
[63] H. J. Schöpe, J. Phys.: Condensed Matter **15**, L533 (2003).
[64] T. Palberg, J. Phys.: Condensed Matter **11**, R323 (1999).